Nuclear Inst. and Methods in Physics Research, A 883 (2018) 33–47

Contents lists available at ScienceDirect

Nuclear Inst. and Methods in Physics Research, A

journal homepage: www.elsevier.com/locate/nima

First optics and beam dynamics studies on the MAX IV 3 GeV storage ring

S.C. Leemann *, M. Sjöström, Å. Andersson

MAX IV Laboratory, Lund University, 22100 Lund, Sweden

A R T I C L E I N F O

Keywords:
Synchrotron light source
Storage ring
Commissioning
Beam injection
Beam characteristics
Beam dynamics

A B S T R A C T

The MAX IV 3 GeV storage ring is the first light source to make use of a multibend achromat lattice to reach ultralow emittance. After extensive commissioning efforts, the storage ring is now ramping up its user program. We present results from beam commissioning of the MAX IV 3 GeV storage ring as well as a summary of the beam dynamics studies that have so for been carried out. We report on injection and accumulation using a single dipole kicker, top-up injection, slow orbit feedback, restoring the linear optics to design, effects of in-vacuum undulators with closed gaps, adjusting nonlinear optics to achieve design chromaticity correction and dynamic aperture sufficient for high injection efficiency and large Touschek lifetime.

Published by Elsevier B.V.

1. Introduction

The MAX IV 3 GeV storage ring is the first light source to make use of a multibend achromat lattice to reach ultralow emittance. First ideas for what would become the MAX IV 3 GeV storage ring were discussed as early as 2002 [1,2] but design efforts intensified during 2006–2009 [3]. Funding for the MAX IV facility was granted in April 2009 and construction started during the summer of 2010. In March 2014, commissioning of the MAX IV linac started with the RF conditioning of the 19 RF stations. Actual beam commissioning of the MAX IV linac started in summer 2014 and lasted until April 2015 when the transfer line to the 3 GeV storage ring was installed. Beam commissioning in the MAX IV 3 GeV storage ring started in August 2015 [4,5]. The MAX IV facility was inaugurated on June 21, 2016 and the first user data was taken in December 2016.

This paper summarizes the events and first results of beam commissioning in the MAX IV 3 GeV storage ring. The next two subsections cover design optics and injection. They are followed by a subsection summarizing the timeline of events during commissioning. The following sections then cover initial injection, orbit measurement and control, linear optics tuning, chromaticity measurement and nonlinear optics tuning, and a few first results concerning emittance, coupling, and lifetime. The final section shall give an overall summary and point out the next studies to be conducted.

1.1. Design optics

The MAX IV 3 GeV storage ring employs a multibend achromat lattice to reach ultralow emittance. An initial lattice was published in [6] and used as the baseline lattice for the Detailed Design Report released in 2010 [3]. This design was later improved and studied in more detail [7–12]. Here we shall not go into any lattice details. Instead, the optics and magnetic lattice are displayed in Fig. 1 and the most important storage ring parameters are summarized in Table 1.

1.2. Injection with a single dipole kicker

The design of the MAX IV 3 GeV storage ring foresees use of a nonlinear kicker magnet for full-energy injection from the MAX IV linac [13]. However, from its inception, this injection was considered too demanding for the first stages of commissioning. Therefore, an injection based on a single dipole kicker was designed [14] and implemented in the MAX IV 3 GeV storage ring. The main idea is to rely on an individual dipole kicker in order to inject both on- and off-axis, as well as to enable accumulation in the storage ring without, however, having to require tight orbit and optics control as in the case of a nonlinear kicker injection scheme. Furthermore, the dipole injection kicker has been installed very close to the injection point (IP) which is defined as the magnetic end of the Lambertson septum, in order to further increase the robustness of injection during initial phases of commissioning.

Details for this injection scheme have been published in [14] and shall not be repeated here. Instead, Fig. 2 shows where the dipole injection kicker is located in the storage ring, as well as the trajectories for the injected and any already stored beam. The dipole injection kicker is excited using a half sine with a base length of 3.5 μs (corresponding to two revolution periods). The situation displayed in Fig. 2 corresponds

* New permanent address: Lawrence Berkeley National Laboratory, Berkeley, CA 94720, USA.
E-mail address: SCLeemann@lbl.gov (S.C. Leemann).

https://doi.org/10.1016/j.nima.2017.11.072
Received 13 October 2017; Accepted 20 November 2017
Available online 2 December 2017
0168-9002/Published by Elsevier B.V.

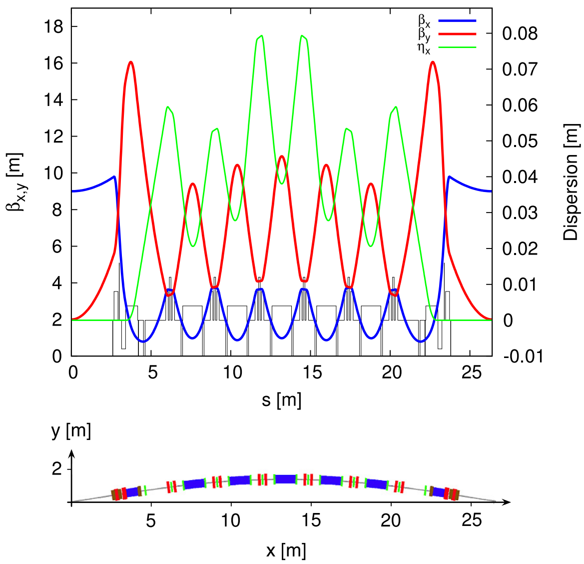

Fig. 1. Design optics in one achromat of the MAX IV 3 GeV storage ring. Top: machine functions. Bottom: magnetic lattice.

Table 1
MAX IV 3 GeV storage ring design parameters.

Stored current I	500 mA
Circumference C	528 m
Main RF f_{rf}	99.931 MHz
Bare lattice emittance ε_0	328 pm rad
Betatron tunes ν_x, ν_y	42.20, 16.28
Linear chromaticity (natural) ξ_x, ξ_y	−50.0, −50.2
Linear chromaticity (corrected) ξ_x, ξ_y	+1.0, +1.0
Linear momentum compaction α_c	3.06×10^{-4}
Energy spread (natural) σ_δ	0.769×10^{-3}
Radiated power (bare lattice) U_0	363.8 keV/turn

to beam accumulation. For initial commissioning, on-axis injection was desired. This can be accomplished by slightly angling the beam at the IP and increasing the injection kick strength.

1.3. Commissioning timeline

Beam commissioning in the MAX IV 3 GeV storage ring started in August 2015 when for the first time electron bunches were guided from the linac extraction area all the way through the 3 GeV transfer line to the Lambertson septum in the storage ring. By August 25 the first turn in the storage ring was recorded and first stored beam was achieved on September 15. First stacking was demonstrated on October 8. This then allowed many orbit and optics studies to be carried out in the bare machine. On November 2 first light was observed on the first diagnostic beamline in the storage ring. By the end of November top-up injection was being applied and the slow orbit feedback (SOFB) loop had been closed.

A first shutdown took place in February 2016 in order to install the first two insertion devices (IDs): two 18 mm period in-vacuum undulators (IVUs) from Hitachi. Once these devices had been commissioned with beam, commissioning of the first two beamlines (frontends, beamline transport, end stations) could be carried out. These two initial beamlines had monochromatic beams at 11 keV in mid May. In June they took first diffraction patterns and by the end of June the gaps had been closed to 4.5 mm. The MAX IV facility was inaugurated on June 21, 2016. During the summer 2016 shutdown the next three IDs were installed: an in-vacuum wiggler (IVW) and two elliptically polarized undulators (EPUs) along with their narrow-gap chambers. By the end of 2016, the two IVU beamlines were routinely taking delivery of 50 mA of

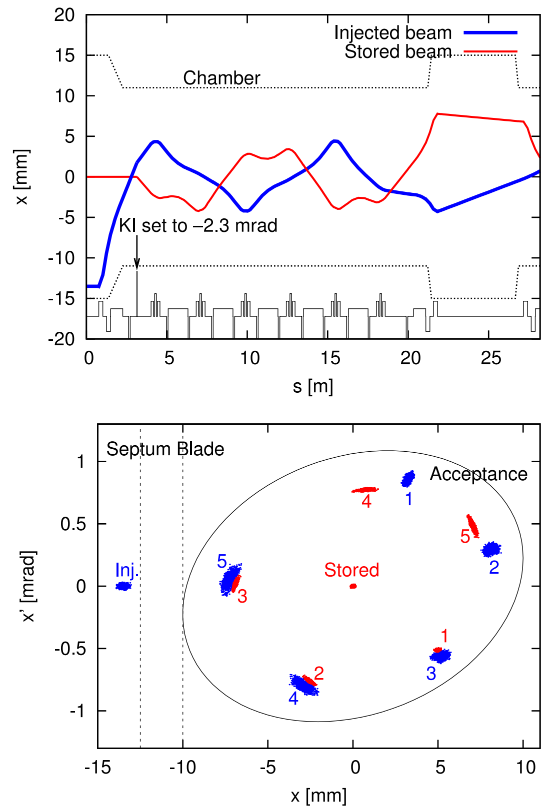

Fig. 2. Accumulation with a single dipole kicker. Top: injection trajectory from end of septum through first achromat with dipole injection kicker (KI) adjusted for accumulation. Bottom: phase space plot at end of septum showing multi-particle tracking data for accumulation case.

beam for beamline commissioning and first experiments, while 198 mA of stored beam had been reached during machine shifts.

This paper will not report on the commissioning of various subsystems as this can be found elsewhere, e.g. [15–21]. The following sections will instead focus entirely on beam commissioning results and tuning efforts.

2. Initial injection & orbit control

Initially, when first electron bunches were guided through the 3 GeV transfer line [13], the signals from the single-pass BPM units installed along the transfer line could be used for beam threading. Once sufficient amounts of charge could be transported all the way to the end of the transfer line, the excitations of the vertical dipoles in the transfer line revealed the extraction energy by fitting to magnetic measurement data. Furthermore, a screen that can be inserted in the high-dispersion area of the transfer line was used to verify the energy spread within and along the individual bunch trains. During this phase, the injector and linac were operating at 0.5 Hz while the RF chopper in the injector area [22–24] was set up to create a roughly 100 ns long bunch train with 500 MHz time structure. This was done in order to increase the signal-to-noise ratio of the BPMs. The linac extraction energy was adjusted to make sure electrons were extracted at 3 GeV to within better than 1%.

The correctors in the transfer line were then adjusted manually in order to decrease the signal on diode rings that had been placed around the vacuum chamber at the downstream end and in the vicinity of the septum. In this way position and angle at the IP were brought closer to design.[1] In a next step, first injections into the storage ring were

[1] One additional BPM was installed right after the injection septum which, together with the first BPM in the storage ring, allows determining the angle at the IP. In practice, however, this was never used.

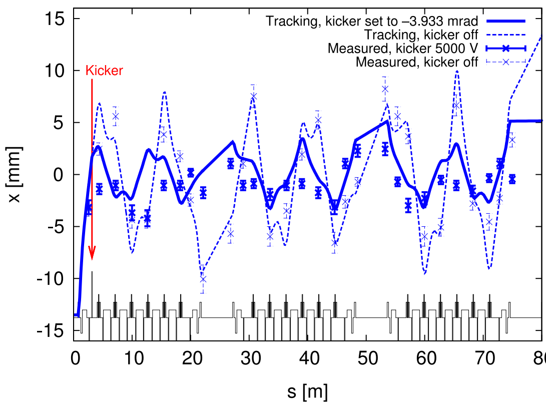

Fig. 3. Electron beam trajectory (with respect to electrical BPM centers) during the first storage ring injections. All magnets at nominal settings and correctors set to zero.

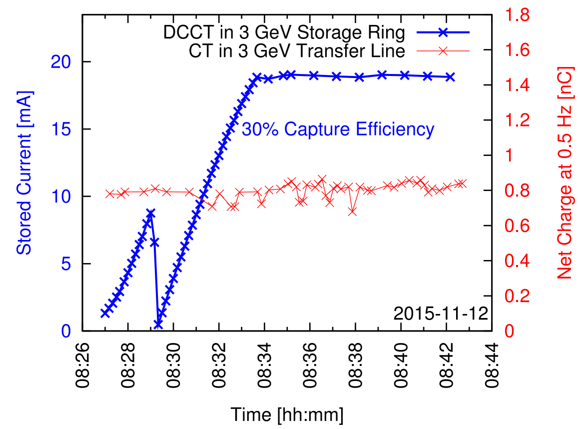

Fig. 5. Current in storage ring (blue) and injected charge per shot from linac transfer line (red) during early stages of commissioning. (For interpretation of the references to color in this figure legend, the reader is referred to the web version of this article.)

attempted. The current transformer (CT) at the end of the transfer line showed a net charge of about 400 pC at 0.5 Hz. One button of the first ring BPM was connected to a high-bandwidth oscilloscope. During these initial injections, this setup revealed a roughly 70 ns train consisting of bunches separated by 2 ns arriving in the storage ring.

2.1. First turns

All magnets in the storage ring had been set to design optics for the bare lattice at 3 GeV [12], i.e. power supply currents according to magnetic measurement data for all magnets [25]. All ring correctors were set to zero. Once the valve downstream of the septum was opened, signal from the beam was detected on all BPMs throughout the first achromat all the way to the position of the next closed valve. One by one valves were then opened and BPM signals could be observed all the way to the 4th long straight (three achromats downstream of the injection, cf. Fig. 3) where the beam appeared to be lost. However, this was the location where beam was expected to be lost when injecting without triggering the injection kicker [14]. At this point the injection kicker was set to ≈ 77% of maximum dipole kicker strength (5 kV corresponding to 3.95 mrad [26]) and then BPM signals appeared also after the 4th long straight.

What then followed was a fairly lengthy radiation survey which required survey data to be taken after opening each additional valve in the ring. After roughly one week, the last valve could be opened and the survey mandated by the commissioning license was complete. Without excitation of a single corrector magnet in the ring and with all other magnets still at their nominal settings, a first turn through the entire storage ring was detected using single-pass data from the ring BPMs (cf. Fig. 4). Using the single-pass BPM data from all ring BPMs and at this point relying only on the electrical BPM centers, this first turn in the ring revealed an rms orbit of 1.35 mm (H) and 1.64 mm (V).

With corrector magnets still zeroed, an attempt was made to shut off all sextupole and octupole magnets. Without the added focusing from these magnets, however, vertical amplitudes increased substantially and the beam was lost in the 11th long straight. The sextupoles and octupoles were brought back to their nominal settings and manual tweaking of transfer line corrector magnets was continued in an attempt to increase the number of turns recorded. For this, the raw ADC buffer of a couple ring BPM buttons was observed in order to count the number of passages and estimate the losses from one turn to another. In this way, first three and later up to 36 turns could be registered.

The effort to further increase the number of turns was interrupted by several technical issues: insufficient cooling water in a dipole power supply, vacuum issues triggered by RF cavity conditioning, and IGBT failure in the pulser of the dipole injection kicker. During the downtime required to resolve these issues, RF cavity conditioning was continued (two out of a total of six cavities are required to store beam). When beam was injected into the storage ring again, manual tweaking of the ring correctors was used to increase the number of turns recorded in the storage ring. During this campaign a misalignment of one of the long straight dummy chambers was detected. The delicate 5-m long Cu vacuum chamber had a ≈ 12 mm kink at its center which was resolved by realignment of the long chamber. Finally, 500 turns in the ring could be detected and a corrector setting for this situation was stored.

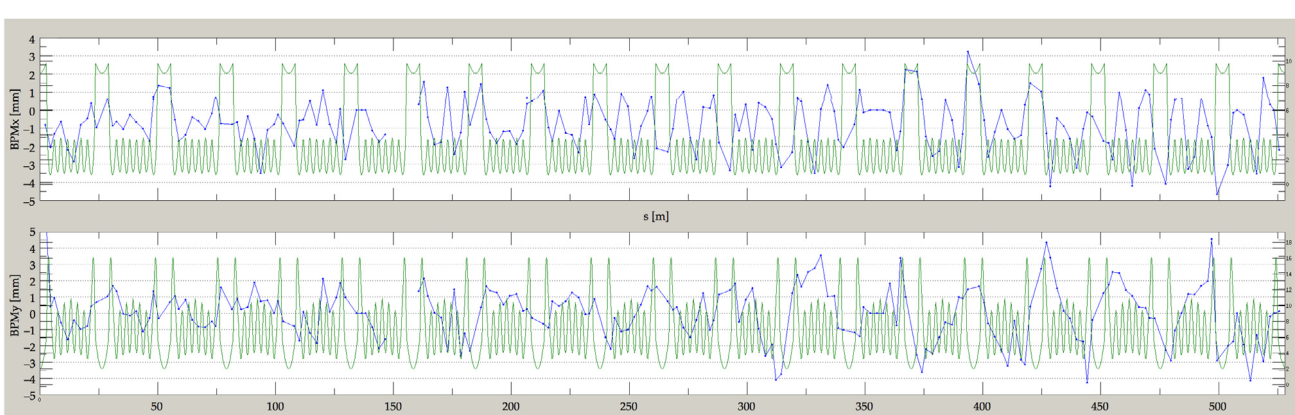

Fig. 4. First turn trajectory (with respect to electrical BPM centers) with all magnets at nominal settings and zeroed correctors. Single-pass BPM data (blue) and design beta functions (green), horizontal (top) and vertical plane (bottom). (For interpretation of the references to color in this figure legend, the reader is referred to the web version of this article.)

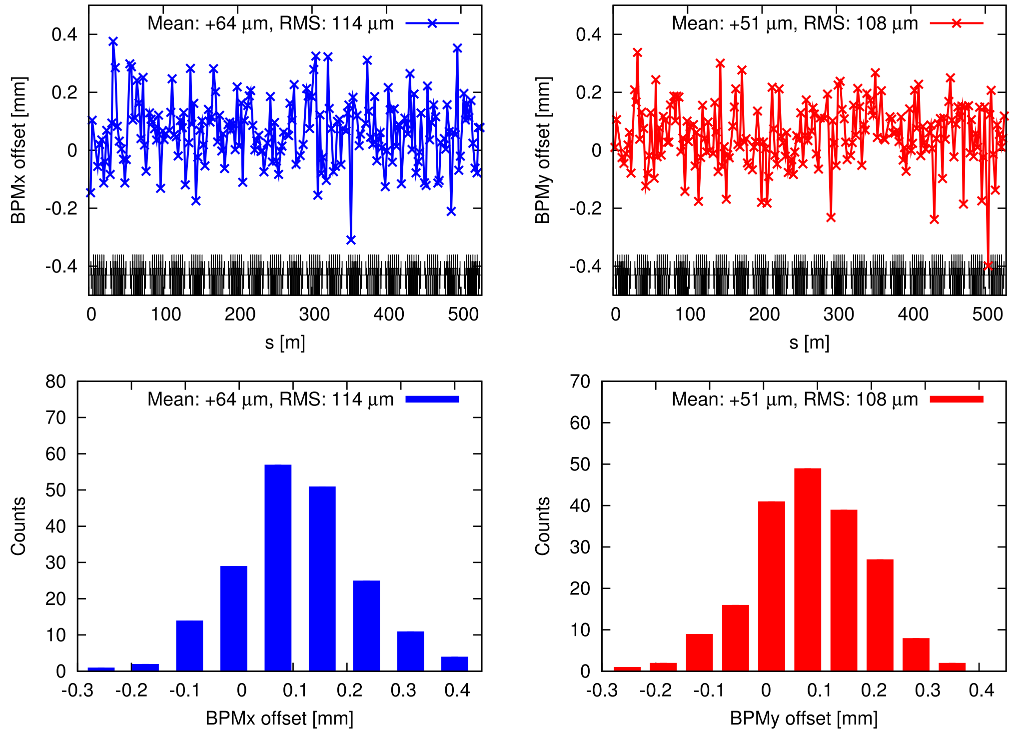

Fig. 6. BPM offset results. Top: measured offsets downloaded to BPM units. Bottom: histogram of BPM offsets.

2.2. Stored beam & RF cavity phasing

With three (out of six) cavities set between 15–20 kW attempts to store beam were made by phasing each cavity individually while observing the stored current signal from the storage ring DC current transformer (DCCT). In the late hours of September 15, 2015 beam was stored for the first time in the MAX IV 3 GeV storage ring. The 0.1 mA recorded by the DCCT corresponded to 170 pC charge remaining in the train injected from the linac. By again using the oscilloscope read-out of one ring BPM button, the bunching process from the original 500 MHz structure (provided by the RF chopper between the thermionic RF gun and first linac section) to the 100 MHz structure of the ring RF system could be observed. The roughly 40 buckets, separated by 2 ns, injected from the linac were observed to bunch into 8 buckets separated by 10 ns over the course of 200 turns (roughly half of the synchrotron period). At this point, the RF chopper in the injector was adjusted to imprint a 100 MHz time structure on the 100 ns bunch train for storage ring injection. By lowering the voltage on the dipole injection kicker, accumulation was then attempted. After some tuning of the working point, during the late hours of October 8, 2015 first stacking to 4.3 mA was observed.

Using one ring BPM connected to a spectrum analyzer the synchrotron tune could be measured. The phases of the three cavities were then tuned individually to maximize the synchrotron tune. Once these relative phases had been determined, the three cavity phases were adjusted coherently with respect to the RF chopper in the injector in order to maximize the injection/capture rate. In this way, it became possible to inject and store several mA of current at a rate of over 4 mA/min which corresponded to a capture efficiency,[2] of about 30%. By November 2015 it was possible to inject and store more than 18 mA in the ring (cf. Fig. 5).

[2] Here capture efficiency is calculated as the ratio of charge stored in the ring after injection is complete, to the charge recorded passing the last CT in the transfer line during injection. This figure therefore does not take into account losses in the injector, linac, or transfer line itself.

2.3. BPM offsets & orbit correction

With a decent injection rate and reliable accumulation in the storage ring established, it was decided to go to the "cold beam limit" at 3 mA and perform first orbit and offset studies with the stored beam. As a prerequisite, the integer tunes were confirmed at their design values 42 (H) and 16 (V) by setting one corrector magnet per plane to a 0.1 mrad kick and then comparing the coherent betatron oscillation recorded around the ring to model data. The design integer tunes had therefore been achieved by simply running all magnets at their nominal settings.

After manual tuning of orbit correctors in small steps, it became possible to keep a stored beam without any excitation of vertical corrector magnets. At this point, an initial attempt was made to determine the BPM offsets. Unlike many 3rd generation storage rings where BPM offsets are determined relative to the adjacent quadrupole, at MAX IV these offsets are calibrated to the magnetic centers of the sextupole or octupole adjacent to the BPM. For this purpose these magnets contain auxiliary coils that can be powered amongst others as an upright quadrupole [12]. A quadrupole centering routine can be applied using the auxiliary coil to determine the magnetic center [27]. The MAX IV approach then assumes that the magnetic center of the sextupole/octupole coincides with the magnetic center of the auxiliary coil on that sextupole/octupole. Using this method, BPM offsets were measured for the entire storage ring using modified routines from MATLAB Middle Layer (MML) [28]. The measured offsets and their distribution are shown in Fig. 6. In the following months these measurements were repeated in order to assess reproducibility, drift, temperature stability, current-dependence, etc.

With BPM offsets determined and downloaded to the Libera Brilliance+ units, the next step was to start correcting the orbit. An example for the corrected orbit along with the distribution of corrector strengths is displayed in Fig. 7. In order to accommodate the vacuum chamber design in the vicinity of the crotch area, there is one BPM per achromat that has only a horizontal corrector magnet instead of a horizontal and vertical pair (each corrector can be powered up to ±5 A, corresponding to roughly ±0.37 mrad). Orbit correction therefore cannot achieve zero vertical orbit in all BPMs in general. Instead, the SVD routine in the

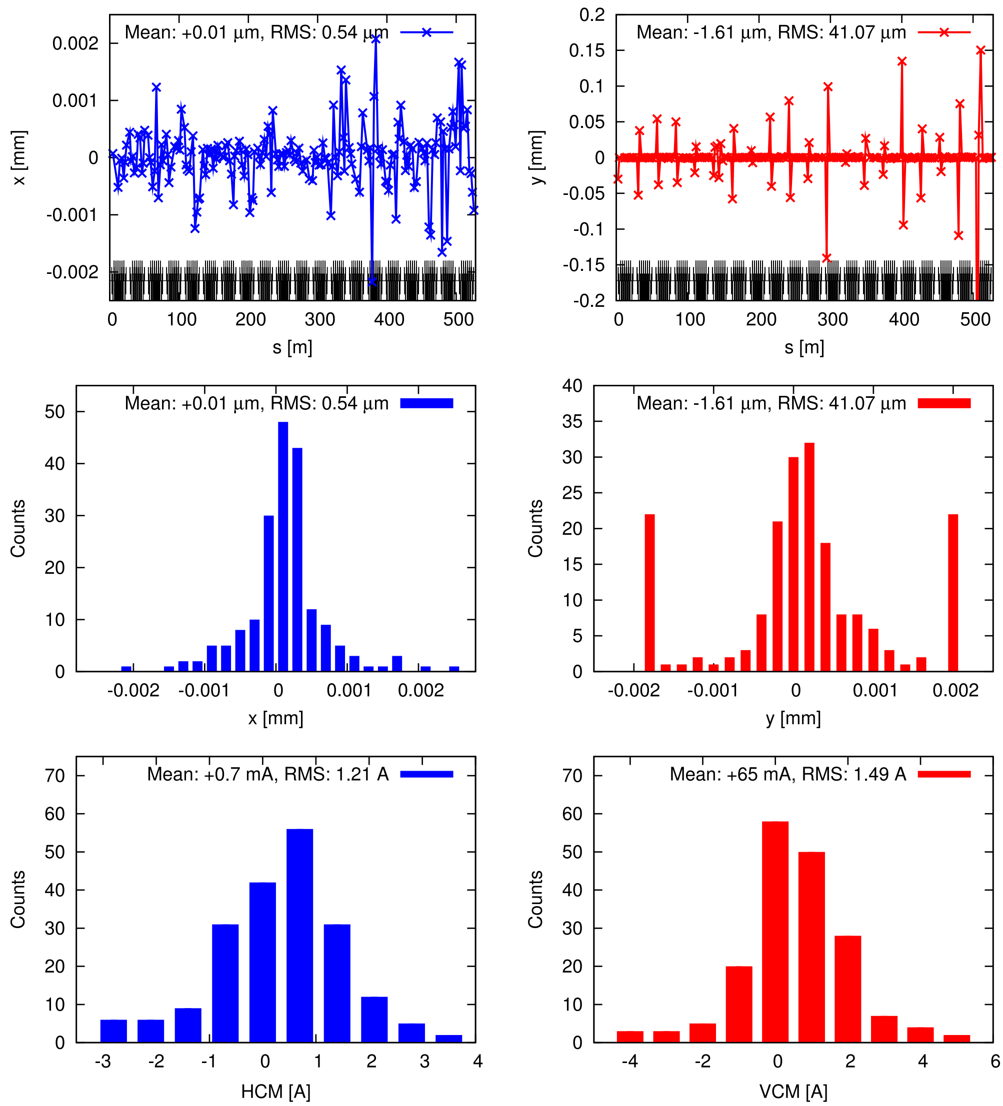

Fig. 7. Orbit correction to downloaded offsets (cf. Fig. 6). Top: closed orbit deviations of corrected orbit. Middle: histogram of closed orbit deviations. Bottom: histogram of required corrector strengths.

applied MML orbit correction has been modified to apply a weighting where orbit errors in BPMs in the long straights (where the IDs are located) are heavily emphasized at the expense of allowing for some vertical orbit excursion throughout the arc. This can be recognized in Fig. 7 where the horizontal orbit is corrected to a sub-micron level rms, while the vertical orbit shows one orbit excursion per achromat in the arc area leading to an overall rms orbit of 41 µm (note also, in the vertical orbit histogram the two columns from larger orbit excursions). Because of the weighting however, across the ID straights, the vertical orbit errors show similarly low values as those observed in the horizontal.

2.4. Accumulation & capture improvements

With a well corrected orbit, injection efficiency started to improve. In order to then raise the level of current that could be injected and stored, the injection kicker pulse length was adjusted. In the initial design the pulser delivers a half-sine with base length equal to two revolution periods (3.5 µs) and amplitude sufficient for on-axis injection (≈ 4.4 mrad) [14,26]. Since during this stage of commissioning on-axis injection was no longer required and considering that accumulation benefits from a reduced perturbation of the stored beam while kicking (which can be achieved by reducing kick amplitude as well as pulse duration [14]), the pulser was modified in such a way as to reduce the pulse length from 3.5 µs to 1.5 µs which also caused a reduction in maximum kick from 5.1 mrad to 2.4 mrad at 6.5 kV. This is very close to the optimum accumulation setting of 2.1 mrad calculated in [14]. Indeed, with this modification of the pulser, optimum injection rates were usually achieved around 5.3 kV corresponding to about 2 mrad.[3]

In addition to these efforts to increase the accumulation rate, the injector and linac settings were also tweaked to maximize the injection efficiency. The RF chopper was adjusted so that no more than 10 consecutive ring buckets were populated per injection shot. Since there is an energy chirp along the bunch train caused by the SLEDs and beam loading in the linac [22–24], the overall train length determines the energy spread across the bunch train. Since the vertical transfer line has a large dispersion and a fairly narrow chamber, it effectively limits the energy acceptance during injection [13].[4] The train length was limited so that losses in the transfer line (i.e. at high energy) were minimized.

[3] This optimum injection kicker strength was later also confirmed for a slightly different working point at 42.14/16.20.

[4] Fairly early during storage ring commissioning a quadrupole polarity error in the transfer line was discovered and resolved. This error had reduced the energy acceptance of the transfer line to only a third of its design value. During an early shutdown the alignment of the magnets in this transfer line was also inspected and improved which led to a further reduction of transfer line losses.

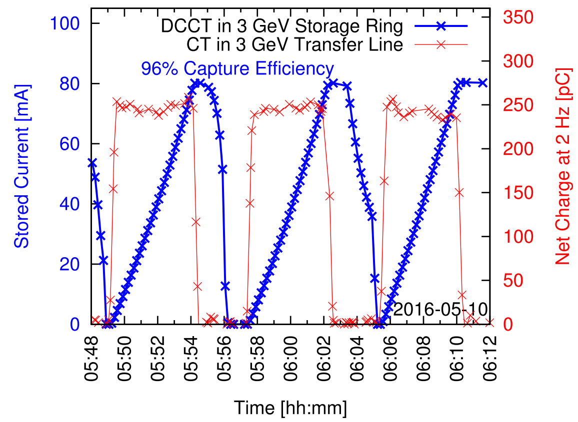

Fig. 8. Current in storage ring (blue) and injected charge per shot from linac transfer line (red) showing increased capture efficiency as commissioning progressed. (For interpretation of the references to color in this figure legend, the reader is referred to the web version of this article.)

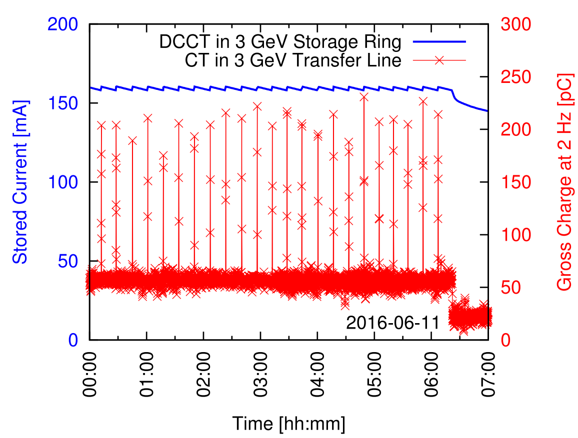

Fig. 9. Stored current (blue) and injected charge per shot from linac transfer line (red) during top-up operation over night. (For interpretation of the references to color in this figure legend, the reader is referred to the web version of this article.)

Furthermore, the RF chopper was adjusted to allow a maximum of three S-band bunches to be injected into each of the ten storage ring buckets per shot. This takes into account the limited phase acceptance of the storage ring at injection [13] and thereby also reduces losses at high energy. Overall, the injector and linac were retuned for good transmission at high energy rather than for maximum charge as had been done during the initial phases of commissioning. With these modifications, very high capture efficiencies could be demonstrated (cf. Fig. 8) and a clear improvement compared to early commissioning was demonstrated (compare Fig. 8 to Fig. 5). With improved capture efficiency and reduced losses, the injection rate could then also be increased from 0.5 Hz to 2 Hz where it remained for the rest of storage ring commissioning (limitation of the commissioning license).

2.5. Top-up injection

In November 2015 top-up injection (albeit with closed shutters since operation was still under commissioning license) was taken into operation. The top-up script that has been developed for this purpose, can initiate injection either according to a pre-defined top-up current deadband or according to a fixed time schedule. An example for an entire night shift with current held constant at 159–160 mA by top-up injection is displayed in Fig. 9.

When the criteria for top-up injection are met, the script automatically adjusts many parameters throughout the facility: the laser to the photogun is blocked on its path to the photocathode,[5] electrons from the thermionic RF gun are allowed to enter the RF chopper and pass the energy filter in the injector on to the linac where they are then accelerated on crest. The injector and linac optics have to be adjusted for ring injection. The extraction dipoles in the appropriate linac extraction area have to be excited to put the beam into the linac septum extraction channel from where the electrons are then transported through the transfer line to the storage ring. Finally, the top-up script has to set the injection kicker to the appropriate voltage and trigger it with the appropriate delays. Once top-up injection is complete (i.e. the required storage ring current threshold has been met), the top-up script returns the linac to SPF injector mode and continues to monitor storage ring current levels.

The top-up script also allows adjusting the desired fill pattern (e.g. to include one or several gaps in the fill pattern or to inject only into a single N-bucket segment of the storage ring[6]), albeit not in a closed-loop feedback mode yet. The bunch pattern is monitored routinely by the oscilloscope signal from a ring BPM button. The charge distribution in the train injected from the linac is not perfectly uniform. Usually the charge delivered to the first and last ring bucket for any given injection shot is lower than the eight buckets populated in between. A simple but effective method to prevent this from imprinting an inhomogeneity onto the fill pattern, is to shift the ring segment into which the next shot will be injected by a value that does not divide the harmonic number h and is different from the length of the injected train. During commissioning a shift of 7 buckets has therefore usually been chosen. This typically results in an even fill pattern even at low stored current, since the amount of charge injected into one bucket during a single top-up shot is usually small compared to the charge already stored in that bucket ($\approx$ 4%).

The top-up script also monitors top-up efficiency. If the amount of injected charge falls below a pre-defined threshold, top-up can be suspended. This can happen when e.g. an RF station trips in the linac or a magnet power supply trips in the transfer line. An example for the former can be recognized in Fig. 9 around 6:20. The top-up script notices an insufficient amount of charge arriving at the storage ring and blocks the thermionic electrons from reaching the linac (note the $\approx$ 200 pC spikes indicating top-up injection shots every 15 min stop appearing after 6:20). In the early version of the top-up script used here, although top-up injection is stopped because of insufficient charge arriving in the transfer line, the injection kicker trigger signal was left on. This is why a more substantial decrease of stored current can be recognized after top-up injection is switched off.

Operational experience with top-up injection has so far been very positive. High amounts of current have been injected into the storage ring and routine use of top-up, especially during hours without commissioning activities, has ensured a strong increase of the accumulated dose [18] and with this increase in dose an improvement of the storage ring vacuum levels and hence lifetime (cf. Section 5). During commissioning so far there have been no signs that accumulation with the single dipole kicker would limit the overall achievable current below the targeted 500 mA. However, for user operation this top-up injection scheme is not suited as it entails significant perturbations of the stored beam while the kicker is triggered [14]. Because of this drawback, the original nonlinear kicker injection scheme was developed [13,31]. As

[5] When the linac is not being used for ring injection it is usually delivering beam to the MAX IV Short Pulse Facility (SPF) [29,30]. In this mode it uses an on-axis photogun as source for the electrons and all linac structures are adjusted to off-crest acceleration in order to create the energy chirp required for magnetic bunch compression.

[6] In principle $N = 1 \ldots h$ where the harmonic number $h = 176$ for the MAX IV 3 GeV storage ring. In practice, however, $N \geq 10$ since the linac usually injects in trains of 10 storage ring buckets. The RF chopper in the thermionic injector area can, however, be modified to inject into a single storage ring bucket if desired [22–24]. During commissioning so far this has been done a few times. Most often, however, when a single-bunch fill of the ring is required, it has been more convenient to fill the usual 10-bucket train into a single storage ring segment and then use the bunch-by-bunch feedback system to clear out all but one bunch.

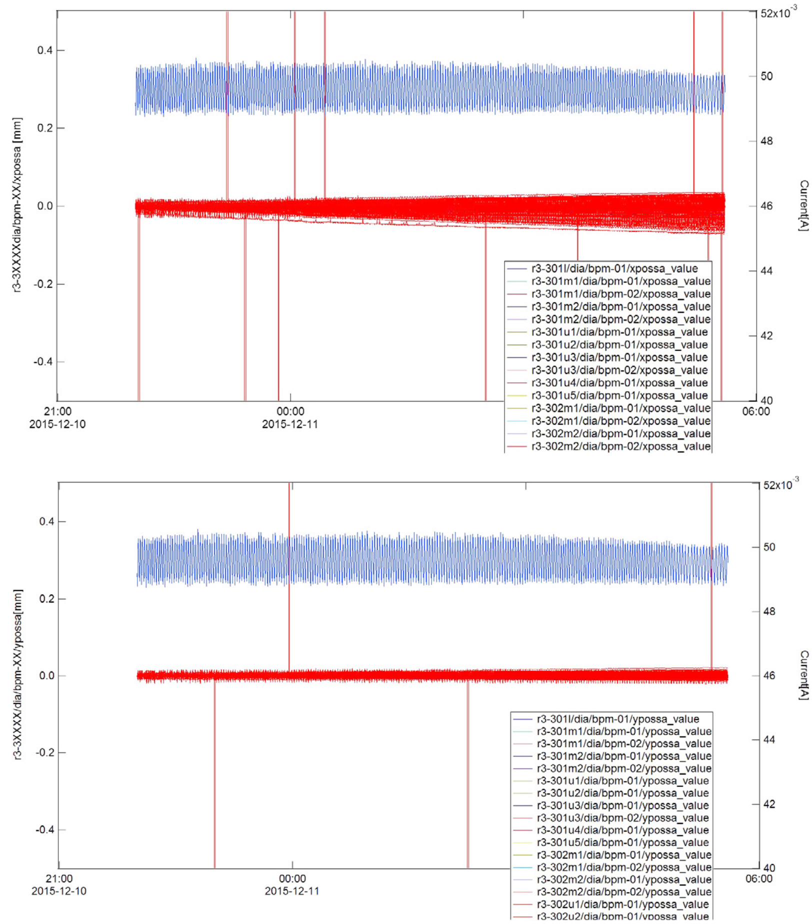

Fig. 10. Drift of BPM readings (red) over a 6-h period (10 Hz data stream, no SOFB running) despite top-up operation ensuring constant current (blue). Top: horizontal BPM readings. Bottom: vertical BPM readings. (For interpretation of the references to color in this figure legend, the reader is referred to the web version of this article.)

soon as the "multipole injection kicker" (MIK) presently being finalized at SOLEIL [32] arrives at MAX IV, commissioning of top-up injection with the MIK will commence. This top-up scheme is expected to be compatible with user operation.

2.6. Slow orbit feedback

Despite top-up injection keeping stored current constant over prolonged periods of time, BPM signals were observed to show both drift and spikes. An example for this is displayed in Fig. 10 showing a period without any orbit feedback. The spikes are randomly distributed among individual BPMs and in time, and are therefore unphysical. Presently, there is a rather clear indication this issue is related to the Tango driver for the Libera Brilliance+. The observed drift, however, is expected due to thermal motion in the storage ring. While most BPMs – in the 10 Hz data stream – show a noise level substantially below 1 μm rms, a considerable drift can be recognized in Fig. 10: about 70 μm (H) and 20 μm (V) over a 6-h period.

This drift in an otherwise very calm machine presents an excellent case for a slow orbit feedback (SOFB). The original MAX IV design foresees both a slow and fast orbit feedback [33]. The SOFB was designed to run at 10 Hz making use of all 380 correctors in the storage ring. In commissioning so far, the SOFB has relied on an MML routine that achieves about 0.5 Hz correction rate. An example for the performance of this SOFB is shown in Fig. 11. The MML SOFB routine iterates the orbit correction procedure described above, hence it preserves the sub-micron correction ability in the horizontal, while in the vertical fulfilling this criterion only in the long straight BPMs.[7] This can be recognized in Fig. 11 (bottom) where horizontal and vertical position readings from ID BPMs clearly show sub-micron stability on the slow time scales the SOFB is intended for. Across individual ID straights orbit stability of 200–400 nm rms (10 Hz data stream) has been measured in both planes when the SOFB loop is closed.

The SOFB can correct towards offsets or a pre-defined golden orbit. The latter has been used to implement bumped orbits during commissioning. Such local bumps in the orbit have been used to characterize the source of hot spots on the vacuum chamber (during ramp-up of the stored current) as well as during ID and beamline commissioning. The SVD-based routine facilitates running the SOFB with disabled BPMs or saturated correctors. Typically, the SOFB relies on ≈ 360 singular values (SVs) which corresponds to the overall number of correctors (200 H, 180 V) minus two or three saturated correctors[8] as well as the number of deactivated BPMs. During most commissioning time, there was a total of roughly a dozen deactivated BPMs. Some had been deactivated because of actual hardware/software issues, others because the BPM had been repurposed, e.g. fill pattern monitor, tune measurement, etc. During commissioning so far, the SOFB has corrected the orbit using a model orbit response matrix (ORM) and correction gain was usually set

[7] This is again a consequence of the lower number of vertical correctors compared to the BPMs as well as the weighting introduced in the orbit correction algorithm.

[8] During much of the commissioning two vertical correctors have shown saturation. It has been possible to run the SOFB nevertheless. However, in the future an alignment check as well as a possible corrector-based realignment [34] are expected to resolve this issue.

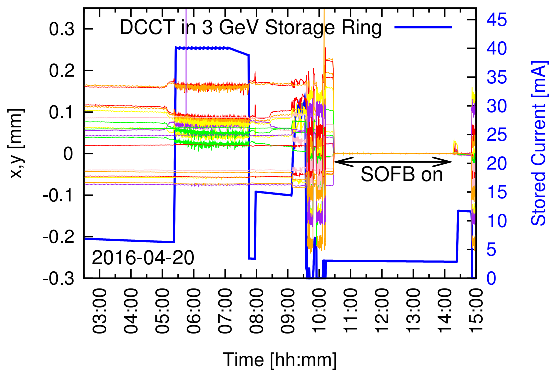

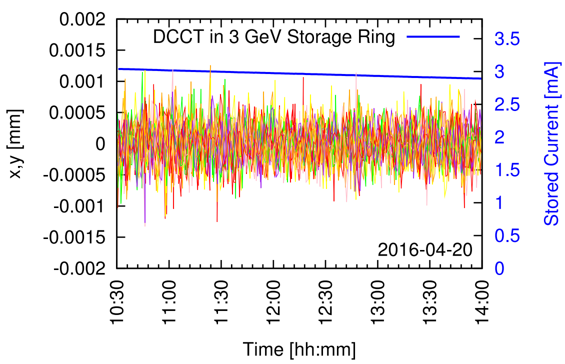

Fig. 11. Position readings from BPMs in ID straights (10 Hz data stream). Top: Results over a 12-h period showing drift during decaying beam, jitter during top-up injection, and stable orbit while the SOFB is running. Bottom: magnified view over the period while the SOFB is running.

to about 30%. Later, during early user operations, a slightly different procedure was followed. The setup was first performed using 360–370 SVs, but then for actual user operations, the SOFB was operated with 140 SVs and gain set to 70%. In this way the feedback becomes more robust to yet unsolved noise issues in the arc BPMs.

During early commissioning, one part of the SOFB routine was not yet running reliably. Whenever a non-zero mean power supply setting was detected for the horizontal correctors, this was an indication that the storage ring RF was not matched to the energy defined by the main dipole fields. In such a situation the ring RF can be adjusted to remove the mean horizontal corrector setting thereby reducing the risk of corrector saturation. Such functionality is built into the SOFB routine used in MML, but at MAX IV could not be used reliably during early commissioning. Fortunately, over the course of a typical beamline commissioning shift the required changes of ring RF are very small (often less than 1 Hz, i.e. $<$ 10 ppb) so it was usually sufficient to adjust the ring RF to remove any mean horizontal corrector settings once at the beginning of a shift by hand. The full range of the orbit corrector power supplies is ± 5 A. At the beginning of a shift the mean horizontal corrector setting is usually removed to better than the 1 mA level. By the end of a shift the mean horizontal corrector strength has rarely grown to more than $\approx$ 20 mA corresponding to a required RF change of roughly 2 Hz. Later, during early user operation, the SOFB routine in MML was adapted to correct in a slightly different manner. It now attempts to adjust the storage ring RF so as to minimize the shift of ring energy from design as calculated from the applied corrector kick strengths. In this way, ring energy shifts during user operations can be maintained below a few hundred eV.

The SOFB has been routinely run during ID and beamline shifts. Not only does it stabilize the beam motion against drift, it protects in-vacuum IDs and ensures the bad-orbit thresholds of the machine protection system (MPS) are not exceeded. These threshold have been derived from ray tracing performed by vacuum experts: above the "cold beam limit" at 3 mA the measured orbit is required to be within ± 0.5 mm of the offset orbit in both planes. Because of the above-mentioned spikes, the MPS does not dump the beam when this limit is exceeded in a single BPM. Instead, the MPS only dumps the beam when five or more BPMs show a bad orbit simultaneously.[9] The exception are the BPM pairs surrounding the in-vacuum IDs. If any of these show a bad orbit, the MPS dumps within 5–50 ms.

3. Linear optics tuning

As indicated in Section 2.3, the integer tunes could be confirmed during early commissioning. With the orbit well corrected, it then became of interest to measure fractional tunes and optical functions. At the time of writing, there exist three independent methods to measure the fractional tunes in the MAX IV 3 GeV storage ring: applying an FFT on turn-by-turn data from BPMs after exciting the beam with the dipole kicker or pinger, using a spectrum analyzer connected to two pairs of striplines as well as a BPM unit (the same unit used to measure the synchrotron tune), as well as the DimTel bunch-by-bunch feedback system which relies on two other pairs of striplines. The latter only became operational during the later stages of commissioning, so the former two methods were used most. Since the kicker and pinger have a half-sine excitation with base length much larger than the 10 ns bunch spacing in the ring, this method works best with a single-bunch or few-bunch fill. Furthermore, because of potentially large amplitude-dependent tune shift, this method is most reliable at low excitation. This method has been implemented as an MML script and can therefore be used online as well as in automated scripts. The spectrum analyzer method, although not automatized yet, requires very little excitation to determine fractional tunes to better than 10^{-3}.

During the early phases of commissioning, magnet families had been adjusted in order to improve injection efficiency or to adjust fractional tunes, but this was done by using MML magnet families. This means, however, that up to this point no balancing or symmetrization of the optics had been carried out.[10] In order to carry out such corrections as well as determine the optical functions, LOCO [35] was performed. At that time, injection into the storage ring usually required a slight shift of RF by about -25 Hz, which rendered tunes around 42.14 and 16.20, respectively. This setting also provided good lifetime. The beta beat was within $\pm 20\%$ (H) and $\pm 25\%$ (V), while the peak horizontal dispersion beating was about $+15/-30$ mm.

The first step of the LOCO-based optics symmetrization consisted of determining the ORM; an example is shown in Fig. 12. Once the ORM had been measured the LOCO fitting could begin. Table 2 shows the parameters of a first LOCO campaign. Note that eleven BPMs have been excluded (due to various issues) as well as one vertical corrector (too close to saturation). The table also reflects that there are fewer vertical than horizontal correctors (cf. Section 2.3). In this first LOCO campaign the goal was to fit BPM gain and coupling[11] as well as power supply settings for all upright quadrupole gradients. These power supply settings are determined by two power supplies per achromat for the two independent horizontally focusing quadrupole families, two power supplies per achromat for the quadrupole doublet flanking every long straight, and finally an additional two power supplies because in long straight no. 8 the two quadrupole doublets are not connected in series.[12]

[9] Since the bad orbit signal to the MPS comes from the Libera Brilliance+ crate and each crate holds electronics for up to four BPMs, two BPMs connected to the same crate showing bad orbit, would technically count as a single bad orbit signal.

[10] During installation of the 140 magnet blocks, blocks were sorted to achieve a smooth distribution of the quadrupole gradients around the ring.

[11] The primary goal of fitting BPM gain and coupling was to verify BPM functionality. In fact, several issues with individual BPMs were discovered in this way and could then be remedied.

[12] The in-vacuum wiggler housed in this straight for the BALDER beamline has been installed at the downstream end of the straight and therefore the local optics matching cannot be done symmetrically [36,37].

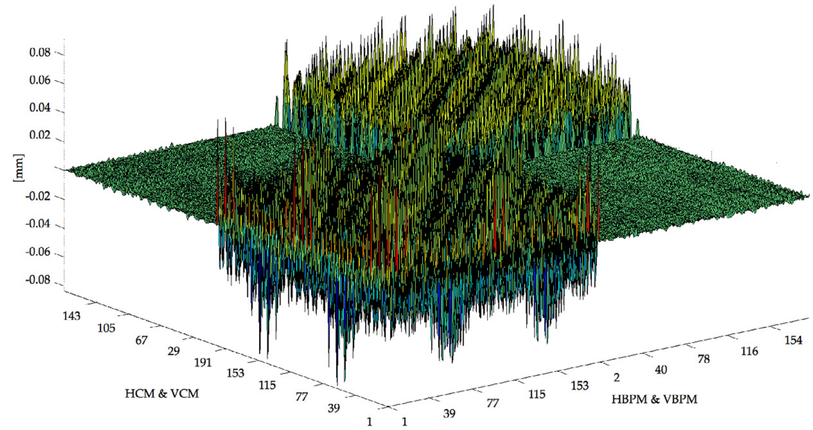

Fig. 12. Plot of measured ORM.

Table 2
Parameters used for uncoupled LOCO fitting.

Parameter type	No. of parameters
BPM gains (H + V)	189 + 189
BPM coupling factors (H + V)	189 + 189
Corrector strengths (H + V)	200 + 179
Corrector coupling factors (H + V)	200 + 179
Dipole gradients (PFSs)	2
Quadrupole gradients	20 × 2 + 20 × 2 + 2

The vertically focusing quadrupole gradients in this storage ring are realized by the transverse gradient in the dipoles which can be tuned by ±4% by exciting pole-face strips (PFSs). Corresponding to the two types of dipoles, there are two families of PFSs and each is connected to one power supply. Because of a deficiency in the design of these PFSs, their excitation not only modifies the transverse gradient in the dipole, but also the dipole field. In order to prevent excitation changes in the PFSs from leading to steering errors that then have to be removed by the orbit feedbacks, a virtual family has been set up in MML. In this manner we compensate for any bend angle changes caused by the PFSs by adjusting the main dipole power supplies.

Since no skew quadrupole gradients were to be fitted in this first LOCO campaign, this is referred to here as "uncoupled" LOCO. It should be noted this campaign made use of an unconstrained LOCO fit, i.e. no penalties were implemented on the parameter changes during fitting [38].

BPM gains are displayed in Fig. 13. The increased BPM gain in BPMs 1 and 8 is the result of a slightly different chamber geometry in the injection area. The ≈ 10% variation among the horizontal BPM gains has so far not been explained. This spread has subsequently proven sensitive to the horizontal dispersion weighting used during fitting, and is therefore not actually considered real. Further refinement of the LOCO configuration is needed.

Fig. 14 shows the singular value (SV) spectrum for the LOCO fit (using the Levenberg–Marquardt algorithm) of the ORM displayed in Fig. 12 according to Table 2 parameters. Only one SV had to be rejected. Finally, Fig. 15 reveals the changes suggested by LOCO for the 84 power supplies which excite upright quadrupole gradients, in order to restore the design optics. It is worth mentioning that this solution is not unique. In particular, when fitting the quadrupole gradients with LOCO this lattice has certain solution modes that have proven very sensitive to noise. One such mode is the triplet consisting of matching cell dipole gradient (adjusted via PFSs), mean QFend gradient, and mean QDend gradient, for which there are many different solutions that give approximately the same phase advance between the same BPM pairs. Another mode, although not as sensitive, is unit cell dipole gradient

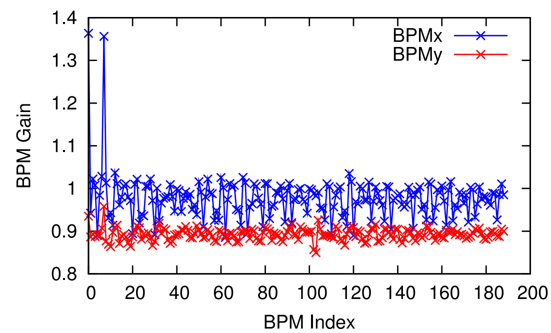

Fig. 13. Uncoupled LOCO results: BPM gain relative to theoretical gain value for standard BPM unit.

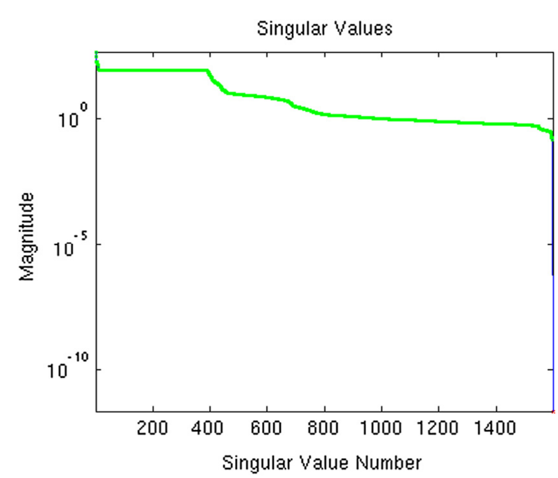

Fig. 14. Spectrum of singular values for the uncoupled LOCO fit. The rejection threshold is at 10^{-6} which leads to a single rejected value (red cross at the bottom right corner). (For interpretation of the references to color in this figure legend, the reader is referred to the web version of this article.)

vs. mean QF and QFm gradients. Hence, unrealistic and out of bounds adjustments of the dipole gradients were often requested in early LOCO fits to symmetrize the lattice. An example of a more realistic adjustment, that was successfully applied to the machine with a corresponding decrease in beta beat, is displayed in Fig. 15. With the present LOCO configuration, noise in the ORM can lead to LOCO solutions with different mean values among the various gradient families. Deviations up to 3% in the mean values of the gradient families have been

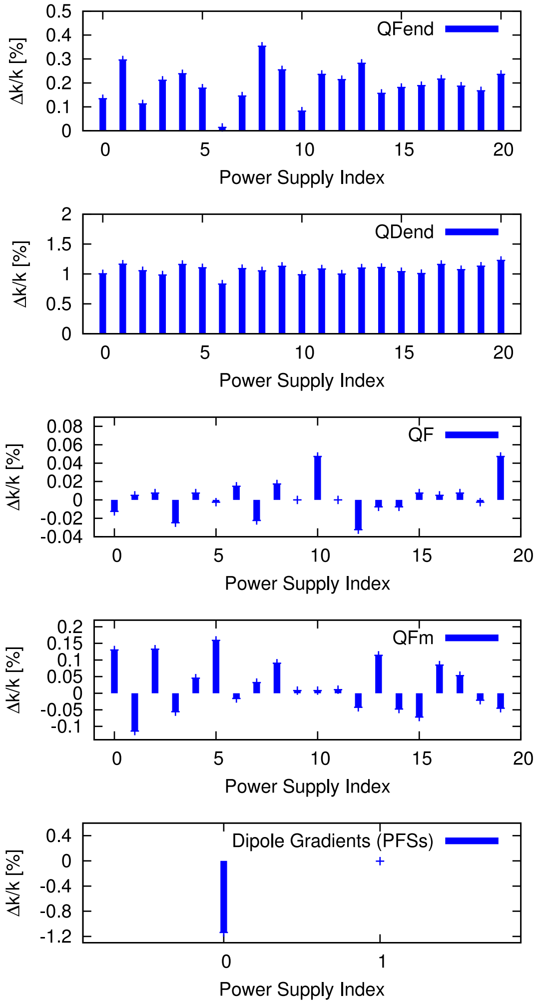

Fig. 15. Required changes to quadrupole gradients according to results of the uncoupled LOCO fit.

observed. No precise conclusions on the average magnetic gradients can therefore be drawn from beam-based measurements yet, other than that they seem to agree to better than 3% compared to direct magnetic measurements. However, as will be shown in the following section, a decent symmetrization can still be achieved with this specific LOCO solution.

Note also, that at this stage, only quadrupole gradient circuits are adjusted. Any imbalance between the gradients of individual quadrupoles connected to the same circuit (e.g. as a result of manufacturing imperfections or cabling) cannot be resolved in this manner. This type of optics symmetrization was foreseen to be carried out in a later stage. For this purpose, each magnet in the magnet block has its own shunt resistor board with modular resistance adjustment. The original idea was that by setting jumpers at the appropriate resistances according to results of a more detailed LOCO fitting campaign, the quadrupole gradients across individual magnets of a family could possibly be further equalized. Later in commissioning, LOCO fits of individual quadrupole gradients were attempted, but not unexpectedly the aforementioned noise sensitivity issues were not ameliorated by increasing the degrees of freedom. Instead, from an operational point of view, the more effective strategy has been to remove dipole gradients from the fit and instead set them to nominal values. This has resulted in a distinct decrease in the noise sensitivity of the LOCO fit along with solutions that have feasible gradient adjustments on the order of 1.5% and still symmetrize the lattice.

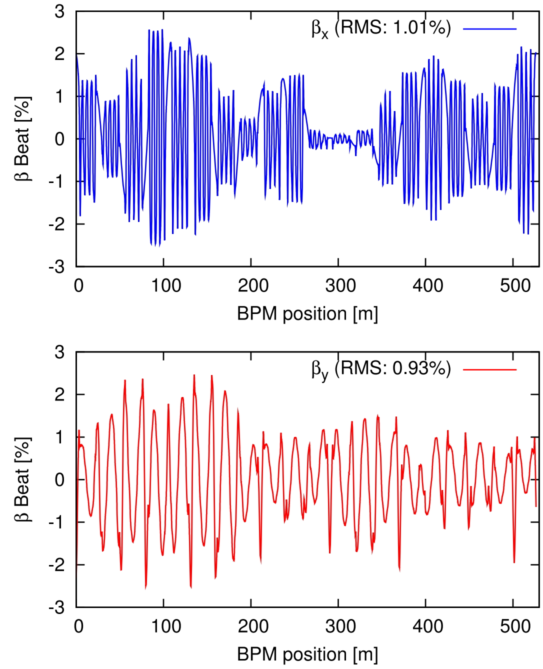

Fig. 16. Remaining beta beat after downloading results of the uncoupled LOCO fit to the quadrupole power supplies: horizontal (top) and vertical (bottom).

3.1. Resulting linear optics

After a couple of iterations of the above mentioned quadrupole gradient circuit symmetrization, the difference between measured ORM and resulting model ORM becomes as low as 0.7 μm rms in both planes, which is not far above the BPM noise level at 3.5 mA. Applying these adjustments to the power supplies results in a correction of the tunes to better than 10^{-2} of their design values, a substantial reduction of beta beating and dispersion beating as well as spurious vertical dispersion. Fig. 16 shows the residual beta beat. In both planes the resulting rms values are around 1% while the maximum observed beta beat is about 2.5%. The residual beating of the horizontal dispersion is displayed in Fig. 17. Although the residual beating of the horizontal dispersion is only 2 mm rms, there also appears to be a systematic offset of -1.2 mm between measurement and design. At the time of writing, it is not yet understood where this comes from.

Finally, the resulting spurious vertical dispersion is shown in Fig. 18. Peak values are 9.5 mm with an rms of 3.5 mm. This spurious vertical dispersion is comparable to the levels observed in tracking studies during the design phase when no skew quadrupole correction was included (in such cases typically $\varepsilon_y \approx 8$ pm rad, i.e. about 2.5% emittance coupling) [9]. When the first measurements of vertical dispersion were performed at the beginning of commissioning, peak values of spurious vertical dispersion as high as 20 mm were observed. During this time residual beating of the horizontal dispersion was also as high as 22 mm. The former could be significantly reduced amongst others by a re-assembly of one defocusing sextupole in which the top half of the magnet had been installed in the magnet block with a longitudinal misalignment of about 2 mm with respect to the bottom half.

3.2. Coupling & effect of insertion devices

In order to further reduce the spurious vertical dispersion as well as suppress coupling, a skew quadrupole correction is required. This resulted from the "coupled" LOCO campaign which was carried out during later stages of commissioning. Results are reported in Section 5.

In commissioning so far, two IVUs have been installed and commissioned. Both are 18 mm period devices from Hitachi with a minimum

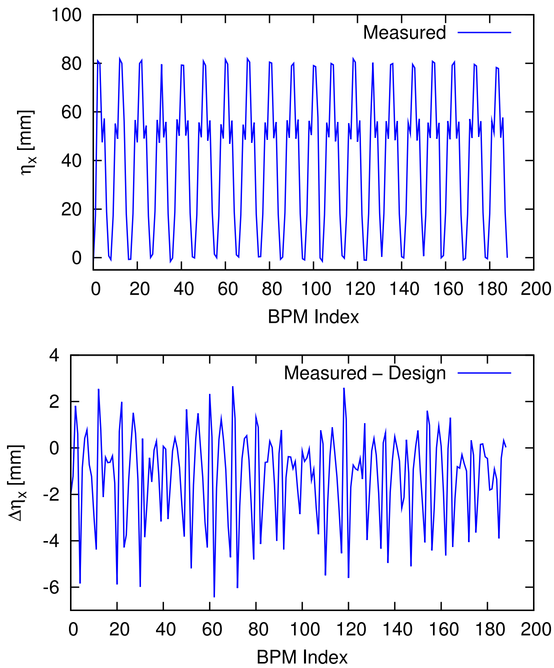

Fig. 17. Horizontal dispersion after downloading results of the uncoupled LOCO fit to the quadrupole power supplies: measured dispersion (top) and dispersion beating (bottom).

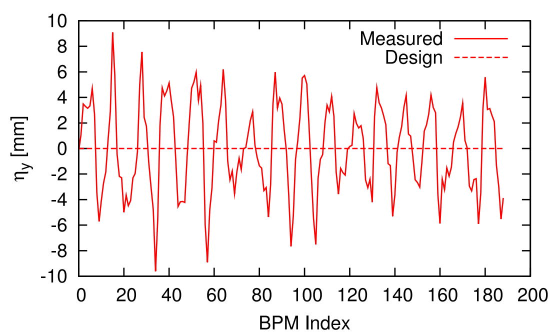

Fig. 18. Spurious vertical dispersion after downloading results of the uncoupled LOCO fit to the quadrupole power supplies. The rms vertical dispersion is 3.5 mm.

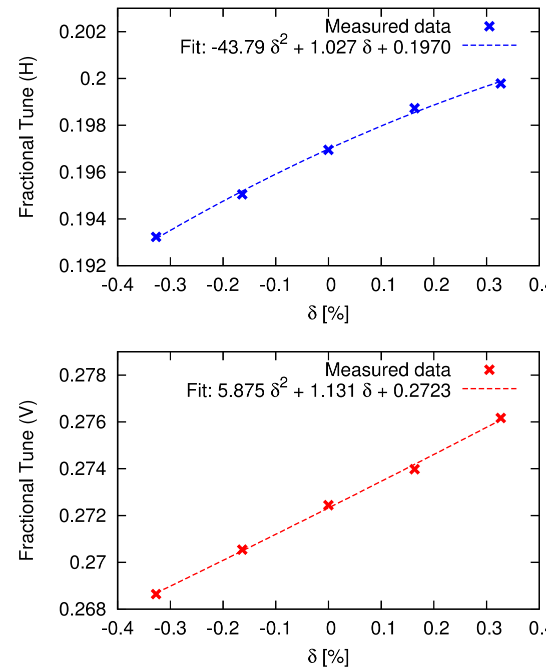

Fig. 19. Measured chromaticity: horizontal (top) and vertical (bottom).

magnetic gap of 4.2 mm and an overall length of just 2 m. Feed-forward tables have been recorded for local correction of first- and second-order field integrals at all gap settings down to 4.5 mm, which is the minimum gap these devices have so far been operated at. During beamline commissioning, application of this feed-forward correction in conjunction with the SOFB has shown to reduce residual orbit deviations to a level of ≈ 1 μm when the gap is closed. However, the feed-forward for the local optics correction as well as the global optics correction (tune feedback) have so far not been operated [36,37]. Nevertheless, no significant change in tune has been observed when closing the gaps of these devices. Since these are short devices and they are not yet being operated at minimum gap, however, the change in vertical tune is expected to be as small as 8×10^{-3} when closing the gap. No signs of beta beating as a result of the not yet operational local optics correction feed-forward has been observed either. For the in-vacuum wiggler and the first two EPUs that are being commissioned next, more significant perturbations of the stored beam are expected.

4. Nonlinear optics tuning

The chromaticity has been determined by measuring the fractional betatron tunes for various ring RF settings. As explained in Section 2.6, the ring RF can be adjusted to ensure it is matched to the energy defined by the main dipole fields. At this point, the RF can be shifted and a corresponding change in associated energy calculated using the model momentum compaction. From this data the chromaticity is then fitted. An example for such a measurement is displayed in Fig. 19. As can be seen from the fit, both linear chromaticities have been corrected to almost their design values of +1. Because of the limited frequency range covered in this measurement as well as the limited number of data points, data has only been fitted up to second order. Within this limited fit, the second-order terms show reasonable agreement with design values at −31 and +8.[13]

After the linear optics had been corrected to a sufficient degree and with the sextupoles and octupoles still at nominal settings, a chromaticity measurement revealed that the linear chromaticities were not both at their design values of +1. While the horizontal chromaticity was very close, in the vertical +3.1 was recorded. Using a simple MML routine, which at this point relied on a model sextupole response matrix, the two strongest chromatic sextupole families SFi and SD were adjusted by about 4% in order to correct the vertical chromaticity. The result of this procedure is the chromaticity displayed in Fig. 19.

4.1. Dynamic acceptance

With both the linear optics corrected to a decent degree and the linear chromaticities close to design values, attention shifted towards the nonlinear dynamics. Scraper measurements have given insight into the lifetime and dynamic acceptance in the storage ring. An initial set of vertical scraper measurements [39] was used to assess various lifetime contributions (see also Section 5) and derive from this the effective pressure the beam encounters at a specific stored current level. Finally, LOCO measurement data for the two magnets directly adjacent to the vertical scraper allowed determination of β_y at the scraper. Together

[13] The design values quoted here were derived by fitting design optics tracking data over the limited fitting range defined by the range of measured data presented here. If fitting of the tracking data is performed using the full $\delta = \pm 5\%$ range and up to fifth order, the corrected second-order chromaticities are −29 and +9, respectively.

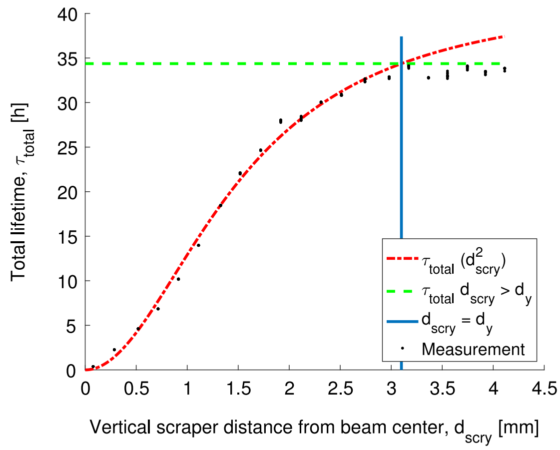

Fig. 20. Vertical scraper measurement at 70 mA. A fit describing total lifetime variation as a function of scraper position is indicated.

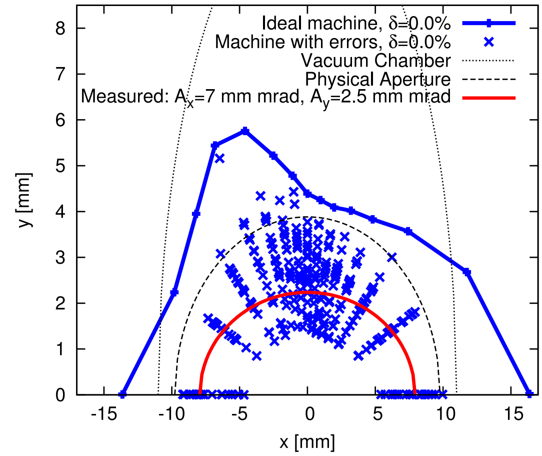

Fig. 21. Comparison of DA simulation results at the center of a long straight (blue) with acceptances determined from scraper measurements (red). (For interpretation of the references to color in this figure legend, the reader is referred to the web version of this article.)

with the scraper's limiting aperture, this allows calculation of the storage ring's vertical acceptance.

An example of such a measurement campaign is displayed in Fig. 20 where total lifetime was measured as a function of the vertical scraper's position at 70 mA. From several measurements, the scraper's limiting aperture, for a magnetic optics close to the one described in Section 3.1 (a minor symmetrization was applied after the Christmas 2016 shutdown), was determined at 3.1 mm. Furthermore, fits of the total lifetime with respect to vertical scraper position for several scraper scans at 70 mA revealed the elastic gas scattering lifetime during April 2017. Assuming the RGA data also reflects the gas composition around the beam, the corresponding pressure encountered by the beam could be determined at $P = 7 \times 10^{-9}$ mbar. However, since the measured rest gas composition is highly hydrogen dominated (around 97%), this pressure result is prone to small changes in the partial pressures of other rest gases and it is prudent to rely solely on lifetime results. The total gas scattering lifetime τ_{gas} at 70 mA during this period was determined at 96 h with an rms error of 4 h. Finally, the Touschek lifetime τ_{ts} contribution can be calculated as the remainder of the overall lifetime. In the example shown in Fig. 20, at 70 mA a total lifetime of 34 h revealed, of which 53 h is Touschek lifetime. During the same measurement, the synchrotron tune was determined at $f_s = 970$ Hz revealing an RF acceptance of $\delta_{rf} = 4.76\%$. A comparison with the measured Touschek lifetime[14] shows that the overall momentum acceptance (MA) δ_{acc} is lower, $3.9 \pm 0.1\%$ (error corresponds to an uncertainty of $\pm 12\%$ on the Touschek lifetime), which indicates that the MA was limited by the lattice.

The vertical beta function at the location of the vertical scraper was determined as $\beta_y = 3.86$ m. Together with the scraper's limiting aperture, this reveals a vertical acceptance in the storage ring of $A_y = 2.5 \pm 0.2$ mm mrad. Similar scraper measurements were also carried out in the horizontal plane. At the location of the horizontal scraper $\beta_x = 9.17$ m and a minimum limiting aperture of 8.0 mm was determined. This reveals a minimum horizontal acceptance of $A_x = 7.0 \pm 0.4$ mm mrad. These dynamic acceptances have been compared to tracking studies carried out during the design phase of MAX IV [9]. An example is displayed in Fig. 21 where dynamic aperture (DA) results for 20 error seeds are shown at the center of an ID straight and compared to the measured acceptances of the storage ring. For the error seeds the tracking studies assumed a storage ring with somewhat increased correlated (girder) misalignment errors as would be expected during early commissioning before a beam-based magnet block realignment campaign [34] is carried out.

[14] During several scraper measurements, the transverse emittances and bunch length were recorded, enabling a comparison with the expected Touschek lifetime.

The measured acceptances of the storage ring appear perfectly compatible with the results from tracking studies. While the vertical acceptance already exceeds what is available when the IVUs or the IVW are operated at closed gaps, the horizontal acceptance does not offer a large margin compared to injection requirements. This result appears to agree with commissioning experience so far, where injection has been quite sensitive to proper dipole kicker excitation. Furthermore, during the first phase of commissioning a slight shift towards lower ring RF (resulting in a decrease of horizontal tune), was always required for good injection efficiency.

Note also, the LOCO campaigns mentioned in Section 3.1 had not been completed entirely in terms of a reduction of spurious vertical dispersion and betatron coupling when the above mentioned scraper measurements were carried out. Indeed, vertical scraper measurements needed to be repeated for several settings of the horizontal scraper to ensure Touschek losses were not collected on the vertical scraper despite the – at this stage – still uncorrected betatron coupling. Once the campaigns to correct betatron coupling and remove vertical dispersion are complete, however, the storage ring acceptance will be remeasured. In addition, pinger studies will be compared to these acceptance measurements and should be able to indicate sources of limited acceptance, if confirmed. Nonlinear tuning by adjusting the three octupole families and/or symmetrization of the five sextupole families (e.g. [40–42]) will then be employed to achieve the storage ring's design performance.

5. Coupling, emittance & lifetime

In a later phase of commissioning the LOCO procedure was repeated, but now also including skew quadrupole correction in order to suppress betatron coupling and spurious vertical dispersion. For this purpose, a maximum of 200 auxiliary coils[15] are available on chromatic sextupoles (160) as well as octupoles without dispersion (40) [12]. The starting point for this campaign was a well corrected orbit[16] and a corrected linear optics following the procedure detailed in Section 3. In a next step, the auxiliary windings on two SFo sextupoles in every achromat are switched to skew quadrupole mode and a LOCO fit including

[15] There are many more such windings installed on all sextupoles and octupoles, but so far, power supplies have only been procured for those 200 magnets that neighbor a BPM.

[16] In this later phase of commissioning one additional vertical orbit corrector per achromat was provided by exciting the auxiliary winding on one SDend sextupole per achromat in vertical corrector mode. This allowed a reduction of orbit excursions in the arc as detailed in Section 2.3. In addition, this has relieved two vertical corrector magnets of the saturation they had been in for most of the early commissioning.

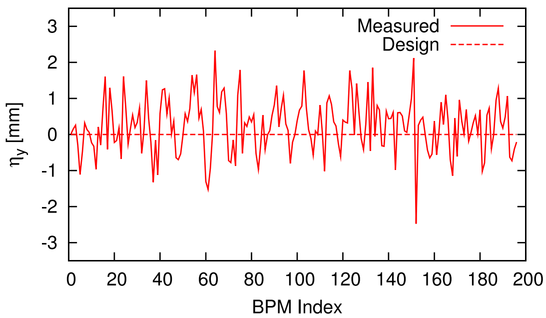

Fig. 22. Spurious vertical dispersion after LOCO correction procedure including skew quadrupole excitation. The resulting rms vertical dispersion is 0.7 mm. This can be compared to the situation before skew quadrupole correction shown in Fig. 18.

the off-diagonal matrices is performed with hard weighting of the vertical dispersion. This fit procedure usually converged very quickly and resulted in a reduction of peak vertical dispersion from around 9.5 mm (3.5 mm rms) to about 2.5 mm (0.7 mm rms). The result of this procedure is shown in Fig. 22. The required excitation of the SFo auxiliary coils used for this vertical dispersion suppression amounts to 27% rms of their peak gradient strength with two outliers using up to 73%.

In a final step we attempt to suppress betatron coupling. For this purpose, the auxiliary windings on the two OXX octupoles in every achromat are switched to skew quadrupole mode and a LOCO fit[17] including the off-diagonal matrices is performed, this time however, without attempting to fit the dispersion. The result is suppression of betatron coupling demonstrated by a reduction of the off-diagonal elements in the ORM (cf. Fig. 23). The excitation of the OXX auxiliary coils in skew quadrupole mode has at this point required about 14% rms of their maximum gradient strength with the largest required gradient amounting to one third of the peak gradient strength. However, although the resulting rms of the ORM coupling quadrants can be reduced from $\approx 13\,\mu$m (after the above-mentioned vertical dispersion correction) to $\approx 8\,\mu$m, this resulting level is comparable to the level initially determined after "uncoupled" LOCO. In this sense, although betatron coupling has been reduced, it cannot be considered fully suppressed. At the time of writing, this remains an ongoing campaign. So far, these coupling and vertical dispersion corrections have not led to unacceptably low lifetime. Should however, during future iterations of this procedure, the resulting emittance coupling become so low that it affects lifetime too severely, a series of successive vertical dispersion bumps will be used to recuperate Touschek lifetime while setting the emittance at the level required by the beamlines [43].

During early commissioning several emittance measurements [44] were carried out using the first diagnostic beamline B320B on the MAX IV 3 GeV storage ring. This diagnostic beamline is still under commissioning, however, first results indicated $\epsilon_y = 6.4 \pm 0.9$ pm rad (from σ- and π-polarized light at 488 nm [45]) and $\epsilon_x = 339 \pm 30$ pm rad (from σ-polarized light at 488 nm [46] whereby the error corresponds to the maximum due to possible systematics). This corresponds to an emittance coupling of $\kappa = 1.9\%$. However, under various initial measurement conditions, emittance coupling as high as $\kappa = 4.6\%$ has also been observed. As long as betatron coupling is not fully suppressed, substantial beam twist is also possible, which can skew apparent vertical emittance results at the diagnostic beamline. Indeed, the latest emittance measurements after minimizing spurious vertical dispersion and suppressing betatron coupling as detailed above, have revealed vertical emittance around 2 pm rad ($\sigma_y = 6 - 6.5\,\mu$m at the diagnostic beamline).

As commissioning progressed, especially once top-up injection to higher stored current became possible (cf. Section 2.5), the accumulated dose quickly increased. Together with this increasing accumulated dose, a continuous reduction of normalized average pressure P_{av}/I has been observed in the storage ring [18], where P_{av} is the average pressure reported by all installed vacuum gauges. This pressure reduction is only briefly interrupted after shutdowns in which vacuum components have been exchanged or installed (e.g. EPU chambers, stripline installation, RF cavity exchange, etc.), after which it resumes to reduce again with increasing accumulated dose. The latest exponential fit of the vacuum conditioning at 160 A h of beam dose reveals

$$P_{av}/I\,[\text{mbar/mA}] = 2 \times 10^{-10} \left(\int I\,dt\,[\text{A h}] \right)^{-0.846}. \tag{1}$$

This pressure reduction with increasing dose shows no signs of saturation so far, indicating the vacuum conditioning of the NEG-coated copper vacuum system is still ongoing [21].

With the improving vacuum, an increase in total lifetime has been observed. Whereas initial commissioning work at a few mA usually took place around $I\tau = 0.3$ A h, commissioning shifts in late 2016 routinely took place at 2–3 A h lifetime. With the above mentioned scraper measurements (cf. Section 4.1), it was possible to separate the different lifetime contributions. The total gas lifetime was determined as 96 ± 4 h at 70 mA in April 2017 (accumulated beam dose at that time was 150 A h). It is interesting to compare the gas lifetime–current product $I\tau_{gas} = 6.7$ A h to the rough design value of 10 A h. Assuming the pressure is dominated by beam-induced desorption, another 100 A h of accumulated beam dose would be required to reach the design target (at $A_y = 2.5$ mm mrad).

[17] No BPM or corrector coupling was included in this fit as the ORM coupling quadrant appearance contains wave patterns indicating optics coupling due to skew components dominates.

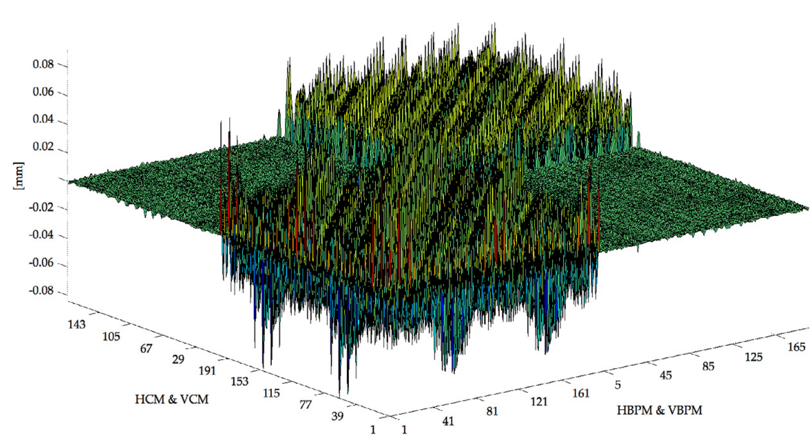

Fig. 23. Measured ORM after skew quadrupole correction of betatron coupling and spurious vertical dispersion.

Apart from the pressure reduction associated with improving vacuum, a clear increase of lifetime as a result of bunch lengthening from tuning of the passive harmonic cavities has been observed [19]. Since three such passive cavities have been installed in the storage ring, achieving flat potential conditions requires ≈ 150 mA of stored beam. Since a significant fraction of commissioning work has occurred below that level, the observed bunch lengthening (typically a factor 2 if stability in all planes is maintained) is not quite as high as anticipated at 500 mA according to design.

6. Conclusions & outlook

Beam commissioning in the MAX IV 3 GeV storage ring has progressed quite far. Injection with a single dipole kicker has proved robust and allowed injection and accumulation of up to 200 mA at high capture efficiency. Orbit correction and symmetrization of the linear optics have been successfully carried out. Top-up injection and SOFB are operated routinely and have allowed ID and beamline commissioning to make progress up to the point where actual user data is being acquired at the first two IVU beamlines.

In terms of MAX IV technology choices, beam commissioning experience so far indicates, that the MAX IV magnet technology using an integrated design relying on solid iron magnet blocks as well as the MAX IV vacuum system relying almost entirely on a narrow water-cooled NEG-coated copper tube, are well performing systems able to satisfy the requirements of the ultralow-emittance lattice based on a multibend achromat design. The relative ease with which first turns and stored beam were achieved indicate excellent alignment provided by magnet integration in blocks as well as laser tracker alignment of the blocks. Furthermore, field quality in the magnet blocks so far appears more than adequate to enable a quick startup.

The next beam commissioning step will be nonlinear optics tuning (in conjunction with pinger measurements as well as experimental frequency map analysis) in order to improve the dynamic acceptance of the storage ring and thereby the lifetime. Furthermore, individual magnets in magnet circuits can be shunted using modular resistances in case optics symmetrization indicates this is indeed required to achieve design performance. Similarly, beam-based magnet block realignment can be applied to relieve corrector strength and achieve better orbit control [34]. Local and global optics matching to IDs will also be employed in order to enable strong IDs to operate in a fashion that is transparent to other users on the ring [36,37]. By enabling online display of transverse beam size (rendering an online transverse emittance monitor) and bunch length measurements from the two diagnostic beamlines, significant improvements in terms of optics adjustments, RF cavity tuning, and ID compensation should become possible. Furthermore, with an online emittance monitor and bunch length measurement as well as higher single-bunch currents, verification of IBS models as well as experimental investigation of IBS and Touschek lifetime at ultralow emittance and medium energy [47] will for the first time become possible. Commissioning of three additional beamlines is underway and during this process we also hope to enable top-up injection with closed ID gaps. Finally, first studies of instabilities and collective effects as well as commissioning of the bunch-by-bunch feedback system have started; first results have been reported in [48].

Once these most important steps in beam commissioning have been taken, there still remain several exciting challenges ahead. A fast orbit feedback system shall be commissioned (fast correctors are already installed) to achieve the 200 nm orbit stability required by the design even at frequencies around 100 Hz and in spite of varying ID gaps and phases. In connection with the suppression of betatron coupling and spurious dispersion, exciting closed vertical dispersion bumps away from the ID straights [43] remains an interesting option to pursue in order to achieve best lifetime at a certain required vertical emittance. Furthermore, with such dispersion bumps ensuring good lifetime, the emittance coupling can be reduced from the original design target of 8 pm rad to 2 pm rad which is expected to significantly increase the brightness for a typical MAX IV IVU beamline [31]. Along this line of reasoning, we hope to be able to also experiment with a harder focusing optics designed to further increase photon brightness and coherence from IDs installed in this storage ring [49–51] to ensure MAX IV remains competitive as other MBA-based storage rings come online.

Acknowledgments

The authors are grateful for the extensive support received from the MAX IV operators during measurement campaigns. Jason Brudvik is acknowledged for his help with the Archiver. Jens Sundberg's scraper measurement data and lifetime analysis are much appreciated. The authors would like to acknowledge Mikael Eriksson, Hamed Tarawneh, and Johan Bengtsson for many stimulating discussions as well as Les Dallin (CLS) for proofreading of the manuscript. The authors would also like to offer their gratitude to the entire MAX IV commissioning team as well as several colleagues from other labs who joined the commissioning effort.

References

[1] M. Eriksson, The MAX4 accelerator system, unpublished internal note, 2002. Available at http://www.maxiv.lu.se/publications.
[2] H. Tarawneh, M. Eriksson, L.-J. Lindgren, B. Anderberg, Nucl. Instrum. Methods A 508 (2003) 480.
[3] MAX IV detailed design report. Available at http://www.maxiv.lu.se/publications.
[4] S.C. Leemann, First commissioning experience with the MAX IV 3 GeV storage ring, Presentation given at the 5th Low Emittance Rings Workshop, ESRF, Grenoble, France, September 2015. https://indico.cern.ch/event/395487/.
[5] S.C. Leemann, Commissioning Progress at the MAX IV 3 GeV Storage Ring, Presentation given at the 6th Low Emittance Rings Workshop, SOLEIL, Paris, France, October 2016. https://indico.cern.ch/event/574973/.
[6] S.C. Leemann, et al., Phys. Rev. ST Accel. Beams 12 (2009) 120701.
[7] S.C. Leemann, A. Streun, Phys. Rev. ST Accel. Beams 14 (2011) 030701.
[8] S.C. Leemann, THPC059, Proceedings of IPAC2011, San Sebastián, Spain, 2011. pp. 3029–3031.
[9] S.C. Leemann, MAX-lab internal note 20121107. Available at http://www.maxiv.lu.se/publications.
[10] S.C. Leemann, The MAX IV 3 GeV storage ring lattice, in: Y. Cai (Ed.) Contribution to ICFA Beam Dynamics Newsletter No. 57 (Section 3.2), pp. 25–35, 2012. http://icfa-bd.kek.jp/Newsletter57.pdf.
[11] P.F. Tavares, S.C. Leemann, M. Sjöström, Å. Andersson, J. Synchrotron Radiat. 21 (2014) 862–877.
[12] S.C. Leemann, Lattice design for the MAX IV storage Rings, in: J. Gao (Ed.) Contribution to ICFA Beam Dynamics Newsletter, No. 71, (Section 5.2), 2017, pp. 188–213. http://icfa-bd.kek.jp/Newsletter71.pdf.
[13] S.C. Leemann, Phys. Rev. ST Accel. Beams 15 (2012) 050705.
[14] S.C. Leemann, Nucl. Instrum. Methods A 693 (2012) 117.
[15] M. Eriksson, et al., MOYAA01, Proceedings of IPAC2016, Busan, Korea, 2016. pp. 11–15.
[16] M. Johansson, MAX IV 3 GeV ring magnets, Presentation given at the 2nd Advanced Low Emittance Rings Technology (ALERT) Workshop, ELETTRA, Trieste, Italy, September 2016. https://indico.cern.ch/event/518497/.
[17] L. Malmgren, MAX IV RF systems, Presentation given at the 2nd Advanced Low Emittance Rings Technology (ALERT) Workshop, ELETTRA, Trieste, Italy, September 2016. https://indico.cern.ch/event/518497/.
[18] E. Al-Dmour, MAX IV vacuum system, from design to operation, Presentation given at the XXIV European Synchrotron Light Source Workshop, MAX IV, Lund, Sweden, November 2016. https://indico.maxiv.lu.se/event/191/.
[19] G. Skripka, et al., WEPOW035, Proceedings of IPAC2016, Busan, Korea, 2016. pp. 2911–2913.
[20] M. Sjöström, MAX IV subsystem commissioning, Presentation given at the 6th Low Emittance Rings Workshop, SOLEIL, Paris, France, October 2016. https://indico.cern.ch/event/574973/.
[21] E. Al-Dmour, M.J. Grabski, The vacuum system of MAX IV storage rings: Installation and conditioning, in: WEPVA090, Proceedings of IPAC2017, Copenhagen, Denmark, 2017.
[22] D. Olsson, et al., Nucl. Instrum. Methods A 759 (2014) 29.
[23] D. Olsson, et al., MOP106015, Proceedings of the 28th Linear Accelerator Conference, LINAC 16, East Lansing, MI, USA, 2016.
[24] J. Andersson, et al., Nucl. Instrum. Methods A 855 (2017) 65.
[25] M. Johansson, et al., TUPMB023, Proceedings of IPAC2016, Busan, Korea, 2016. pp. 1157–1159.
[26] Final Design Report: Dipole kickers for MAX IV, The Budker Institute of Nuclear Physics, unpublished, 2013.

[27] G. Portmann, D. Robin, L. Schachinger, RPQ13, Proceedings of 1995 Particle Accelerator Conference, Dallas, TX, USA, 1995. pp. 2693–2695.
[28] J. Corbett, G. Portmann, A. Terebilo, WPPE020, Proceedings of the 2003 Particle Accelerator Conference, Portland, OR, USA, 2003. pp. 2369–2371.
[29] S. Werin, et al., Nucl. Instrum. Methods A 601 (2009) 98.
[30] S. Thorin, et al., Proceedings of the 2011 Particle Accelerator Conference, New York, NY, USA, 2011. pp. 2447–2449.
[31] S.C. Leemann, L.O. Dallin, WEPSM05, Proceedings of PAC2013, Pasadena, CA, USA, 2013. pp. 1052–1054.
[32] S.C. Leemann, Pulsed multipole injection for the MAX IV storage rings, Presentation given at the 5th Low Emittance Rings Workshop, ESRF, Grenoble, France, September 2015. https://indico.cern.ch/event/395487/.
[33] M. Sjöström, et al., MOPO010, Proceedings of IPAC2011, San Sebastián, Spain, 2011. pp. 499–501.
[34] M. Sjöström, et al., Nucl. Instrum. Methods A 597 (2008) 170.
[35] J. Safranek, et al., WEPLE003, Proceedings of EPAC 2002, Paris, France, 2002. pp. 1184–1186.
[36] E. Wallén, S.C. Leemann, TUP235, Proceedings of the 2011 Particle Accelerator Conference, New York, NY, USA, 2011. pp. 1262–1264.
[37] S.C. Leemann, H. Tarawneh, TUPJE038, Proceedings of IPAC2015, Richmond, VA, USA, 2015. pp. 1696–1698.
[38] X. Huang, J. Safranek, LOCO with constraints and improved fitting technique, SLAC-PUB-13686, 2009.
[39] J. Sundberg, Touschek- and gas scattering lifetime investigations in the MAX IV 3 GeV storage ring, in: Synchrotron Radiation Based Science, Lund University, AX IV Laboratory, Faculty of Science, 2017 (Master's thesis).
[40] R. Bartolini, et al., Phys. Rev. ST Accel. Beams 11 (2008) 104002.
[41] R. Bartolini, et al., Phys. Rev. ST Accel. Beams 14 (2011) 054003.
[42] J. Bengtsson, et al., Phys. Rev. ST Accel. Beams 18 (2015) 074002.
[43] J. Breunlin, S.C. Leemann, Å. Andersson, Phys. Rev. Accel. Beams 19 (2016) 060701.
[44] J. Breunlin, Emittance related topics for fourth generation storage ring light sources, Lund University, 2016 (Doctoral thesis). http://lup.lub.lu.se/record/a21733df-070d-4c1d-afcf-bc9c273ff243.
[45] J. Breunlin, Å. Andersson, WEPOW034, Proceedings of IPAC2016, Busan, Korea, 2016. pp. 2908–2910.
[46] J. Breunlin, Å. Andersson, MAX IV 3 GeV ring emittances: Diagnostics based on near-visible synchrotron radiation, Presentation given at the XXIV European Synchrotron Light Source Workshop, MAX IV, Lund, Sweden, November 2016. https://indico.maxiv.lu.se/event/191/.
[47] S.C. Leemann, Phys. Rev. ST Accel. Beams 17 (2014) 050705.
[48] G. Skripka, Beam instability measurements and analysis in the MAX IV 3 GeV storage ring, Presentation given at the 6th Low Emittance Rings Workshop, SOLEIL, Paris, France, October 2016. https://indico.cern.ch/event/574973/.
[49] S.C. Leemann, M. Eriksson, TUPRI026, Proceedings of IPAC2014, Dresden, Germany, 2014. pp. 1615–1617.
[50] S.C. Leemann, First upgrade ideas for the MAX IV 3 GeV storage ring, Presentation given at the 2nd Low Emittance Ring Lattice Design Workshop, MAX IV, Lund, Sweden, December 2016. https://indico.maxiv.lu.se/event/193/.
[51] S.C. Leemann, W.A. Wurtz, Pushing the MAX IV 3 GeV storage ring brightness and coherence towards the limit of its magnetic lattice, in: WEPAB002, Proceedings of IPAC2017, Copenhagen, Denmark, 2017.